Localization with monostatic ISAC system: LOS detection and parameter estimation

Jiamin Long*, Le Zheng*, Marco Lops†, Fan Liu‡, Chuanhao Zhao*
E-mail: jiaminlong0548@163.com, le.zheng.cn@gmail.com, lops@unina.it, liuf6@sustech.edu.cn, 13041258366@163.com
*School of Information and Electronics, Beijing Institute of Technology, Beijing 100081, China
†Department of Electrical and Information Technology, University of Naples Federico II, 80138 Naples, Italy
‡Department of Electronic and Electrical Engineering, Southern University of Science and Technology, Shenzhen 518055, China

***Abstract*—In this paper, we address the Line-of-Sight (LOS) localization problem in a monostatic Integrated Sensing and Communication (ISAC) system based on colocated Multiple-Input Multiple-Output (MIMO) technology in the presence of multipath scenarios. Firstly, we derive Generalized Likelihood Ratio Tests (GLRTs) to distinguish LOS paths from Non-Line-of-Sight (NLOS) paths based on full-rank and rank-deficient transmit waveform, providing closed-form expressions for false alarm probability and detection probability. Furthermore, in the case of unknown path parameters, we employ the GLRT philosophy, utilizing meticulously developed estimators to replace the unknown parameters. The angular parameters of both LOS and NLOS paths are estimated using a sparsity-enforced Compressed Sensing (CS) approach, aiming at estimating angular parameters in the continuous domain. Finally, we compare the performance of full-rank and rank-deficient waveforms in different scenarios and demonstrate the effectiveness of the proposed detection-estimation solution through simulations.**

***Index Terms*—ISAC, multipath, LOS detection.**

I. Introduction

In recent years, Integrated Sensing and Communications (ISAC) has garnered significant research attention due to its potential as a compelling solution for integrating sophisticated radar sensing functionalities seamlessly into the existing cellular infrastructure [1]. Colocated Multiple-Input Multiple-Output (MIMO) technology has become integral to ISAC systems, offering a multitude of advantages. For sensing purposes, colocated MIMO systems can create virtual arrays using a relatively small number of antenna elements, thus offering enhanced precision in target angle estimation [2]. This capability enhances the precision of target localization and tracking, contributing to the overall efficacy of ISAC in diverse scenarios. Furthermore, in the context of communication, colocated MIMO introduces a valuable attribute by offering more degrees of freedom (DOF) in signaling strategies [3]. This increased DOF allows for the exploitation of the propagation channel in a manner that enhances communication performance, making colocated MIMO a pivotal technology for both sensing and communication aspects within ISAC systems.

Traditional ISAC-based solutions typically assume a simple Line-of-Sight (LOS) channel, but real-world ISAC systems encounter more complex multipath scenarios [4]. In real-world scenarios, Non-Line-of-Sight (NLOS) paths are relatively abundant. Usually, range gating can effective in eliminate NLOS paths from the target under detection, owing to variations in propagation delays. However, for NLOS paths, signal reflections from multiple surfaces result in the breakdown of the assumption in colocated MIMO systems that the direction of departure (DOD) equals the direction of arrival (DOA). This fact can lead to a degradation in the performance of traditional angle estimation [5]. Therefore, the LOS paths of intended targets might be affected by NLOS paths from unrelated objects. Effectively extracting LOS information from the densely distributed NLOS environment becomes a crucial challenge for optimizing the performance of ISAC systems.

In some distributed systems, such as cooperative base stations [6] and distributed MIMO radar [7], the extraction of LOS paths and target localization typically relies on the matching processing of range measurements. However, within the framework of monostatic ISAC systems, LOS extraction cannot be achieved through distance matching. An alternative approach for estimating the number and angles of multipaths is proposed in [8]. This method assumes a single LOS path scenario and utilizes Convolutional Neural Networks (CNNs) for LOS identification and parameter extraction. Another strategy introduced in [9] involves a multipath detection approach employing the Generalized Likelihood Ratio Test (GLRT) to distinguish whether the estimated angles correspond to LOS or NLOS. However, this method is constrained by its assumption of the existence of only one set of multipaths in the scenario. Consequently, these methodologies encounter challenges in achieving precise LOS localization and identification within more complex multipath environments.

In our previous journal paper [10], we proposed a method for identifying ghost targets caused by multipaths, presenting multipath estimation methods alongside a GLRT detection framework for automotive radar. Building upon this foundation, in this paper, we extend our exploration to the application of the GLRT framework for LOS detection and parameter estimation in monostatic ISAC systems. The LOS detection is framed as a binary hypothesis problem: $\mathcal{H}_0$ assumes observations contain only NLOS paths, where DOD and DOA don't coincide, while $\mathcal{H}_1$ suggests the presence of LOS paths with matching DODs and DOAs. To tackle this, we employ the GLRT philosophy to design the detector structure, utilizing

2024 IEEE Radar Conference (RadarConf24) | 979-8-3503-2920-9/24/$31.00 ©2024 IEEE | DOI: 10.1109/RADARCONF2458775.2024.10548681

meticulously developed estimators to replace the unknown parameters. Furthermore, this paper extends our previous work [10] by analyzing ISAC waveform characteristics, including both full-rank and rank-deficient waveforms, to deepen our understanding of LOS detection capabilities in ISAC systems and their performance implications. The effectiveness of the proposed strategy is evaluated through simulations, providing validation for the robustness and efficacy of the approach.

II. Signal Model

In this paper, we consider a colocated MIMO array with M_T transmitter antennas and M_R receiver antennas. The signal transmitted by m-th TX is

$$\chi_m(t) = \sum_{l=0}^{L} x_m(l)\xi(t-(l-1)T), \tag{1}$$

where T denotes frame repetition time, each frame having the same duration $T_c = T/Q, Q \in \mathbb{N}$. $x_m(l)$ denotes the m-th transmitted symbol in the l-th time spot, L is the code length. The $\xi(\cdot)$ represents a transmit signal that satisfies the Nyquist criterion with respect to T_c, where the bandwidth is $1/T_c$, and Q range cells are defined [11].

Given the presence of multiple reflecting objects within the field of view, LOS paths from intended targets may be compromised by NLOS paths originating from other unrelated reflecting objects. Assuming there are K_0 LOS paths and K_1 NLOS paths present in the q-th range cell, i.e. they hit receiver with time delay qT_c, thus generating echoes at time instants $\{qT_c + (l-1)T\}_{l=1}^{L}$. Denoting $\boldsymbol{\chi}(t) = [\chi_1(t-qT_c), \chi_2(t-qT_c), \ldots, \chi_{M_T}(t-qT_c)]^T$, the signal returned form q-th range cell of n-th receiver antenna can be written as

$$\begin{aligned} y_n(t) &= \sum_{k=1}^{K_0} \alpha_k \upsilon_n(\theta_k)\mathbf{a}_T^T(\theta_k)\boldsymbol{\chi}(t) + w_n(t) \\ &+ \sum_{k=1}^{K_1} \left(\alpha'_{1,k}\upsilon_n(\vartheta_k)\mathbf{a}_T^T(\varphi_k)\boldsymbol{\chi}(t) + \alpha'_{2,k}\upsilon_n(\varphi_k)\mathbf{a}_T^T(\vartheta_k)\boldsymbol{\chi}(t)\right), \end{aligned} \tag{2}$$

where $\mathbf{a}_T(\theta) = \frac{1}{\sqrt{M_T}}\left[1, e^{j\frac{2\pi d\sin(\theta)}{\lambda}}, \ldots, e^{j\frac{2\pi d(M_T-1)\sin(\theta)}{\lambda}}\right]^T$ denotes the transmitter steering vector with input angle θ; λ denote the wavelength; d is the inter-antenna element spacing with $d \geq \lambda/2$; $\{\alpha_k\}_{k=1}^{k=K_0}$ and $\{\alpha'_{k,1}, \alpha'_{k,2}\}_{k=1}^{k=K_1}$ are the complex reflection coefficients of k-the LOS path and k-th pair NLOS paths, respectively; $\upsilon_n(\theta) = e^{\frac{j2\pi d(n-1)\sin(\theta)}{\lambda}}$ denotes the response of n-th receiver to the angle θ; θ_k represents the DOD for the k-th LOS path, which coincides with the DOA; ϑ_k and φ_k denote the DOD and DOA, respectively, for the k-th pair of NLOS paths, where $\vartheta_k \neq \varphi_k$; $w_n(t)$ constitutes spatially uncorrelated, zero-mean, complex Gaussian noise.

To derive the discrete-time representation of observations, we project $y_n(t)$ onto a set of orthogonal functions $\xi(t-qT_c-(l-1)T)_{l=1}^{L}$, i.e.,

$$\begin{aligned} y_{n,l} &= \langle y_n(t), \xi(t-qT_c-(l-1)T)\rangle \\ &= \sum_{k=1}^{K_0} \alpha_k \upsilon_n(\theta_k)\mathbf{a}_T^T(\theta_k)\mathbf{x}(l) + w_{n,l} \\ &+ \sum_{k=1}^{K_1} \left(\alpha'_{1,k}\upsilon_n(\vartheta_k)\mathbf{a}_T^T(\varphi_k)\mathbf{x}(l) + \alpha'_{2,k}\upsilon_n(\varphi_k)\mathbf{a}_T^T(\vartheta_k)\mathbf{x}(l)\right), \end{aligned} \tag{3}$$

where $\langle y(t), q(t)\rangle$ is defined as the integral of the product of $y(t)$ and the complex conjugate of $q(t)$ over the entire real line, given by $\int_{-\infty}^{\infty} y(t)q^*(t)dt$; $w_{n,l} = \langle w_n(t), \xi(t-qT_c-(l-1)T)\rangle$, $\mathbf{x}(l) = [x_1(l), \cdots, x_{M_T}(l)]^T \in \mathbb{C}^{M_T\times 1}$ denotes the coded waveform at the l-epoch.

The discretization process can equivalently be represented by the common practice in radar receivers of performing matched filtering using a filter matched to the pulse waveform $\xi(t)$, followed by sampling at the inverse of the bandwidth T_c. Denoting $\mathbf{w}(l) = [w_{1,l}, \cdots, w_{M_R,l}]^T \in \mathbb{C}^{M_R\times 1}, \mathbf{y}(l) = [y_{1,l}, \cdots, y_{M_R,l}]^T \in \mathbb{C}^{M_R\times 1}$, we have

$$\begin{aligned} \mathbf{y}(l) &= \sum_{k=1}^{K_0} \alpha_k \mathbf{a}_R(\theta_k)\mathbf{a}_T^T(\theta_k)\mathbf{x}(l) + \mathbf{w}(l) \\ &+ \sum_{k=1}^{K_1} (\alpha'_{k,1}\mathbf{a}_R(\varphi_k)\mathbf{a}_T^T(\vartheta_k) + \alpha'_{k,2}\mathbf{a}_R(\vartheta_k)\mathbf{a}_T^T(\varphi_k))\mathbf{x}(l) \\ &= (\mathbf{H}_{\text{LOS}} + \mathbf{H}_{\text{NLOS}})\mathbf{x}(l) + \mathbf{w}(l), \end{aligned} \tag{4}$$

where $\mathbf{H}_{\text{LOS}} = \sum_{k=1}^{K_0} \alpha_k \mathbf{a}_R(\theta_k)\mathbf{a}_T^T(\theta_k)$ and $\mathbf{H}_{\text{NLOS}} = \sum_{k=1}^{K_1}\left(\alpha'_{k,1}\mathbf{a}_R(\varphi_k)\mathbf{a}_T^T(\vartheta_k) + \alpha'_{k,2}\mathbf{a}_R(\vartheta_k)\mathbf{a}_T^T(\varphi_k)\right)$ represent the channel response of LOS paths and NLOS paths, respectively; $\mathbf{a}_R(\cdot) \in \mathbb{C}^{M_R\times 1}$ is the steering vectors of receiver array with the form of $\mathbf{a}_R(\theta) = \frac{1}{\sqrt{M_R}}\left[1, e^{j2\pi d\sin(\theta)/\lambda}, \ldots, e^{j2\pi(M_R-1)d\sin(\theta)/\lambda}\right]^T$, where θ denotes the angle input of $\mathbf{a}_R(\cdot)$.

Denoting $\boldsymbol{\theta} = [\theta_1, \theta_2, \ldots, \theta_{K_0}] \in \mathbb{R}^{K_0}$, $\boldsymbol{\vartheta} = [\vartheta_1, \vartheta_2, \ldots, \vartheta_{K_1}] \in \mathbb{R}^{K_1}$, $\boldsymbol{\varphi} = [\varphi, \varphi, \ldots, \varphi_{K_1}] \in \mathbb{R}^{K_1}$, $\boldsymbol{\alpha} = [\alpha_1, \alpha_2, \ldots, \alpha_{K_0}]^T \in \mathbb{C}^{K_0\times 1}$, $\boldsymbol{\alpha}' = [\alpha'_{1,1}, \ldots, \alpha'_{K_1,1}, \alpha'_{1,2}, \ldots, \alpha'_{K_1,2}]^T \in \mathbb{C}^{2K_1\times 1}$, we have

$$\mathbf{H}_{\text{LOS}} = \mathbf{A}_R(\boldsymbol{\theta})\boldsymbol{\Lambda}\mathbf{A}_T^T(\boldsymbol{\theta}), \tag{5}$$

$$\mathbf{H}_{\text{NLOS}} = \mathbf{A}_R(\boldsymbol{\psi}_r)\boldsymbol{\Lambda}'\mathbf{A}_T^T(\boldsymbol{\psi}_t), \tag{6}$$

where $\boldsymbol{\psi}_r = [\boldsymbol{\varphi}; \boldsymbol{\vartheta}]$, $\boldsymbol{\psi}_t = [\boldsymbol{\vartheta}; \boldsymbol{\varphi}]$, $\boldsymbol{\Lambda} = \text{diag}(\boldsymbol{\alpha})$, $\boldsymbol{\Lambda}' = \text{diag}(\boldsymbol{\alpha}')$, $\mathbf{A}_T(\boldsymbol{\theta})$ and $\mathbf{A}_R(\boldsymbol{\theta})$ denote the steering matrices of the radar TX and RX arrays with the input angle set $\boldsymbol{\theta}$

$$\mathbf{A}_T(\boldsymbol{\theta}) = [\mathbf{a}_T(\theta_1), \mathbf{a}_T(\theta_2), \ldots, \mathbf{a}_T(\theta_{K_0})] \in \mathbb{C}^{M_T\times K_0},$$
$$\mathbf{A}_R(\boldsymbol{\theta}) = [\mathbf{a}_R(\theta_1), \mathbf{a}_R(\theta_2), \ldots, \mathbf{a}_R(\theta_{K_0})] \in \mathbb{C}^{M_R\times K_0}.$$

The $\mathbf{A}_T(\boldsymbol{\psi}_t)$ and $\mathbf{A}_R(\boldsymbol{\psi}_r)$ share the same form, with the input angle set $\boldsymbol{\theta}$ being replaced by $\boldsymbol{\psi}_t$ and $\boldsymbol{\psi}_r$, respectively. Denote $\mathbf{X} = [\mathbf{x}(1), \cdots, \mathbf{x}(L)]$ as space-time code-matrix, $\mathbf{W} = [\mathbf{w}(1), \cdots, \mathbf{w}(L)]$, we obtain

$$\begin{aligned} \mathbf{Y} &= [\mathbf{y}(1), \cdots, \mathbf{y}(L)] \in \mathbb{C}^{M_R\times L} \\ &= (\mathbf{H}_{\text{LOS}} + \mathbf{H}_{\text{NLOS}})\mathbf{X} + \mathbf{W}, \end{aligned} \tag{7}$$

where $\mathbf{W}$ is additive white Gaussian noise with zero mean and variance σ^2.

III. Detection and localization

A. Detector design

1) Full-rank waveform: Consider $\mathbf{X}$ is pilot waveform with full-rank characteristics and we use a set of M_T matched filters each matched with one of M_T transmitting waveforms to extract signals corresponding to each TX-RX pair

$$\begin{aligned}\mathbf{Z} &= \mathbf{Y}\mathbf{X}^H \in \mathbb{C}^{M_R\times M_T}\\ &= (\mathbf{H}_{\mathrm{LOS}}+\mathbf{H}_{\mathrm{NLOS}})\mathbf{X}\mathbf{X}^{\mathrm{H}}+\mathbf{W}\mathbf{X}^{\mathrm{H}}.\end{aligned} \tag{8}$$

We vectorize $\mathbf{Z}$ to obtain

$$\begin{aligned}\mathbf{z} &= \mathrm{vec}((\mathbf{H}_{\mathrm{LOS}}+\mathbf{H}_{\mathrm{NLOS}})\mathbf{X}\mathbf{X}^{\mathrm{H}}+\mathbf{W}\mathbf{X}^{\mathrm{H}})\\ &= (\mathbf{X}^*\mathbf{X}^T\otimes\mathbf{I}_{M_R})(\mathbf{A}_{\mathrm{LOS}}\boldsymbol{\alpha}+\mathbf{A}_{\mathrm{NLOS}}\boldsymbol{\alpha}')\\ &\quad+(\mathbf{X}^*\otimes\mathbf{I}_{M_R})\tilde{\mathbf{w}},\end{aligned} \tag{9}$$

where $\mathbf{I}_{M_R}$ denotes the $M_R\times M_R$ identity matrix; $\mathbf{A}_{\mathrm{LOS}}=\mathbf{A}_T(\boldsymbol{\theta})\circ\mathbf{A}_R(\boldsymbol{\theta})$, $\mathbf{A}_{\mathrm{NLOS}}=\mathbf{A}_T(\boldsymbol{\psi}_t)\circ\mathbf{A}_R(\boldsymbol{\psi}_r)$ denote the steering matrix of LOS paths and NLOS paths, respectively; $\otimes$ and $\circ$ denote the Kronecker product and Khatri-Rao (KR) product, respectively.

Defining $\mathbf{R}_x=\mathbf{X}^*\mathbf{X}^T$, $\mathbf{r}=(\mathbf{X}^*\otimes\mathbf{I}_{M_R})\tilde{\mathbf{w}}$, $\boldsymbol{\beta}_0=\boldsymbol{\alpha}'$, $\boldsymbol{\beta}_1=[\boldsymbol{\alpha}^T,(\boldsymbol{\alpha}')^T]^T$, $\mathbf{A}_0=\mathbf{A}_{\mathrm{NLOS}}$ and $\mathbf{A}_1=[\mathbf{A}_{\mathrm{LOS}},\mathbf{A}_{\mathrm{NLOS}}]$, we formulate the problem of LOS detection as a binary hypothesis test as follows

$$\begin{aligned}\mathcal{H}_0:&\quad \mathbf{z}=(\mathbf{R}_x\otimes\mathbf{I}_{M_R})\mathbf{A}_0\boldsymbol{\beta}_0+\mathbf{r},\\ \mathcal{H}_1:&\quad \mathbf{z}=(\mathbf{R}_x\otimes\mathbf{I}_{M_R})\mathbf{A}_1\boldsymbol{\beta}_1+\mathbf{r}.\end{aligned} \tag{10}$$

According to the Neyman-Pearson criterion, the optimum solution to the hypotheses testing problem (10) is the likelihood ratio test. In what follows, we introduce and examine a GLRT, operating under the assumption that the number of LOS and NLOS paths, along with their associated angular information—that is, the matrices $\mathbf{A}_{\mathrm{LOS}}$ and $\mathbf{A}_{\mathrm{NLOS}}$—are known. Since

$$\begin{aligned}\mathbb{E}(\mathbf{r}\mathbf{r}^H) &= \mathbb{E}\left((\mathbf{X}^*\otimes\mathbf{I}_{M_R})\tilde{\mathbf{w}}\tilde{\mathbf{w}}^H(\mathbf{X}^*\otimes\mathbf{I}_{M_R})^H\right)\\ &= (\mathbf{X}^*\otimes\mathbf{I}_{M_R})\sigma^2\mathbf{I}_{M_RL}(\mathbf{X}^T\otimes\mathbf{I}_{M_R})\\ &= \sigma^2(\mathbf{X}^*\mathbf{X}^T)\otimes\mathbf{I}_{M_R}\\ &= \sigma^2\mathbf{R}_x\otimes\mathbf{I}_{M_R},\end{aligned} \tag{11}$$

we have $\mathbf{r}\sim\mathcal{CN}(\mathbf{0},\sigma^2\boldsymbol{\Sigma}_x)$ where $\boldsymbol{\Sigma}_x=\mathbf{R}_x\otimes\mathbf{I}_{M_R}$. Because $\mathrm{rank}(\mathbf{R}_x)=\mathrm{rank}(\mathbf{X})=M_T$, the correlation matrix $\boldsymbol{\Sigma}_x$ is also full-rank. The data $\mathbf{z}$ can be whitened by $\boldsymbol{\Sigma}_x^{-1/2}$, the test can be converts to

$$\begin{aligned}H_0:&\bar{\mathbf{z}}\sim\mathcal{CN}(\boldsymbol{\Sigma}_x^{1/2}\mathbf{A}_0\boldsymbol{\beta}_0,\sigma^2\mathbf{I}_{M_TM_R}),\\ H_1:&\bar{\mathbf{z}}\sim\mathcal{CN}(\boldsymbol{\Sigma}_x^{1/2}\mathbf{A}_1\boldsymbol{\beta}_1,\sigma^2\mathbf{I}_{M_TM_R}),\end{aligned} \tag{12}$$

where $\bar{\mathbf{z}}=\boldsymbol{\Sigma}_x^{-1/2}\mathbf{z}$. The maximum likelihood estimates (MLE) of $\boldsymbol{\beta}_0$ and $\boldsymbol{\beta}_1$ can be readily constructed as $\hat{\boldsymbol{\beta}}_0=(\boldsymbol{\Sigma}_x^{1/2}\mathbf{A}_0)^\dagger\bar{\mathbf{z}}$, $\hat{\boldsymbol{\beta}}_1=(\boldsymbol{\Sigma}_x^{1/2}\mathbf{A}_1)^\dagger\bar{\mathbf{z}}$, where $(\cdot)^\dagger$ denotes the pseudo-inversion. Plugging those estimations into likelihood function, we can obtain the MLE of σ^2 under $\mathcal{H}_1$ and $\mathcal{H}_0$ as $\hat{\sigma}_1^2=\frac{1}{M_TM_R}\left\|\bar{\mathbf{z}}-\boldsymbol{\Sigma}_x^{1/2}\mathbf{A}_1\hat{\boldsymbol{\beta}}_1\right\|^2$, $\hat{\sigma}_0^2=\frac{1}{M_TM_R}\left\|\bar{\mathbf{z}}-\boldsymbol{\Sigma}_x^{1/2}\mathbf{A}_0\hat{\boldsymbol{\beta}}_0\right\|^2$, and, as a consequence, the GLRT becomes

$$\mathcal{T}_F=\frac{\hat{\sigma}_0^2}{\hat{\sigma}_1^2}=\frac{\left\|\boldsymbol{P}_0^{\perp}\bar{\mathbf{z}}\right\|^2}{\left\|\boldsymbol{P}_1^{\perp}\bar{\mathbf{z}}\right\|^2}\underset{\mathcal{H}_0}{\overset{\mathcal{H}_1}{\gtrless}}\lambda_G, \tag{13}$$

where $\mathbf{P}_0^{\perp}=\mathbf{I}_{M_TM_R}-\boldsymbol{\Sigma}_x^{1/2}\mathbf{A}_0(\boldsymbol{\Sigma}_x^{1/2}\mathbf{A}_0)^\dagger$ and $\mathbf{P}_1^{\perp}=\mathbf{I}_{M_TM_R}-\boldsymbol{\Sigma}_x^{1/2}\mathbf{A}_1(\boldsymbol{\Sigma}_x^{1/2}\mathbf{A}_1)^\dagger$, λ_G denotes the detection threshold.

2) Rank-deficient waveform : To mitigate the potential impact of unknown reflection coefficients, which may reduce the received signal energy to levels unsuitable for reliable detection [12], the ISAC base station (ISAC-BS) judiciously allocates its total power across various paths using a customized transmit beamforming (TBF) approach. We can express the transmitted waveform as $\mathbf{X}=\mathbf{F}\mathbf{S}$, where $\mathbf{F}=[\mathbf{f}_1,\mathbf{f}_2,\ldots,\mathbf{f}_J]\in\mathbb{C}^{M_T\times J}$ denotes the TBF matrix, $\mathbf{S}\in\mathbb{C}^{J\times L}$ denote the space-time code for J beams. Thus, the receive signal can be rewritten as

$$\mathbf{Y} = (\mathbf{H}_{\mathrm{LOS}}+\mathbf{H}_{\mathrm{NLOS}})\mathbf{F}\mathbf{S}+\mathbf{W}. \tag{14}$$

Generally, the number of transmit beams is less than the number of transmit antennas, so the covariance matrix of the waveform $\mathbf{X}$ is rank-deficient. Hence, we define it as a rank-deficient waveform. We employ matched filtering of the received signal using the transmission signal $\mathbf{S}^H$ and obtain

$$\begin{aligned}\mathbf{Z} &= \mathbf{Y}\mathbf{S}^H\in\mathbb{C}^{M_R\times J}\\ &= (\mathbf{H}_{\mathrm{LOS}}+\mathbf{H}_{\mathrm{NLOS}})\mathbf{F}\mathbf{S}\mathbf{S}^{\mathrm{H}}+\mathbf{W}\mathbf{S}^{\mathrm{H}}\\ &= (\mathbf{A}_R(\boldsymbol{\theta})\boldsymbol{\Lambda}\mathbf{A}_T^T(\boldsymbol{\theta})+\mathbf{A}_R(\boldsymbol{\psi}_r)\boldsymbol{\Lambda}'\mathbf{A}_T^T(\boldsymbol{\psi}_t))\mathbf{F}\mathbf{S}\mathbf{S}^H\\ &\quad+\mathbf{W}\mathbf{S}^H\\ &= (\mathbf{A}_R(\boldsymbol{\theta})\boldsymbol{\Lambda}\mathbf{A}_{TB}^T(\boldsymbol{\theta})+\mathbf{A}_R(\boldsymbol{\psi}_r)\boldsymbol{\Lambda}'\mathbf{A}_{TB}^T(\boldsymbol{\psi}_t))\mathbf{S}\mathbf{S}^H\\ &\quad+\mathbf{W}\mathbf{S}^H,\end{aligned} \tag{15}$$

where $\mathbf{A}_{TB}(\cdot)=\mathbf{F}^T\mathbf{A}_T(\cdot)$ denotes the transmit steering matrix after beamforming. We vectorize $\mathbf{Z}$ to obtain

$$\begin{aligned}\mathbf{z} &= \mathrm{vec}((\mathbf{H}_{\mathrm{LOS}}+\mathbf{H}_{\mathrm{NLOS}})\mathbf{F}\mathbf{S}\mathbf{S}^H+\mathbf{W}\mathbf{S}^H)\in\mathbb{C}^{M_RJ}\\ &= \mathbf{R}_s\otimes\mathbf{I}_{M_R}\left(\widetilde{\mathbf{A}}_{\mathrm{LOS}}\boldsymbol{\alpha}+\widetilde{\mathbf{A}}_{\mathrm{NLOS}}\boldsymbol{\alpha}'\right)\\ &\quad+(\mathbf{S}^*\otimes\mathbf{I}_{M_R})\tilde{\mathbf{w}},\end{aligned} \tag{16}$$

where $\widetilde{\mathbf{A}}_{\mathrm{LOS}}=\mathbf{A}_{TB}(\boldsymbol{\theta})\circ\mathbf{A}_R(\boldsymbol{\theta})$, $\widetilde{\mathbf{A}}_{\mathrm{NLOS}}=\mathbf{A}_{TB}(\boldsymbol{\psi}_t)\circ\mathbf{A}_R(\boldsymbol{\psi}_r)$, $\mathbf{R}_s=\mathbf{S}^*\mathbf{S}^T$. Similarly, we define $\boldsymbol{\Sigma}_{\tilde{s}}=\mathbf{R}_s\otimes\mathbf{I}_{M_R}$, $\tilde{\mathbf{r}}=(\mathbf{S}^*\otimes\mathbf{I}_{M_R})\tilde{\mathbf{w}}$, $\widetilde{\mathbf{A}}_0=\widetilde{\mathbf{A}}_{\mathrm{NLOS}}$ and $\widetilde{\mathbf{A}}_1=[\widetilde{\mathbf{A}}_{\mathrm{LOS}},\widetilde{\mathbf{A}}_{\mathrm{NLOS}}]$. The hypothesis testing problem is rewritten as follows

$$\begin{aligned}\mathcal{H}_0:&\quad \mathbf{z}=(\mathbf{R}_s\otimes\mathbf{I}_{M_R})\widetilde{\mathbf{A}}_0\boldsymbol{\beta}_0+\tilde{\mathbf{r}},\\ \mathcal{H}_1:&\quad \mathbf{z}=(\mathbf{R}_s\otimes\mathbf{I}_{M_R})\widetilde{\mathbf{A}}_1\boldsymbol{\beta}_1+\tilde{\mathbf{r}}.\end{aligned} \tag{17}$$

Denote $\tilde{\mathbf{z}} = \mathbf{\Sigma}_s^{-1/2}\mathbf{z}$, $\widetilde{\mathbf{P}}_0^{\perp} = \mathbf{I}_{M_T M_R} - \mathbf{\Sigma}_s^{1/2}\widetilde{\mathbf{A}}_0(\mathbf{\Sigma}_s^{1/2}\widetilde{\mathbf{A}}_0)^{\dagger}$ and $\widetilde{\mathbf{P}}_1^{\perp} = \mathbf{I}_{M_T M_R} - \mathbf{\Sigma}_s^{1/2}\widetilde{\mathbf{A}}_1(\mathbf{\Sigma}_s^{1/2}\widetilde{\mathbf{A}}_1)^{\dagger}$, we follow the derivation for the full-rank waveform and obtain the GLRT as:

$$\mathcal{T}_R = \frac{\left\|\widetilde{\boldsymbol{P}}_0^{\perp}\tilde{\mathbf{z}}\right\|^2}{\left\|\widetilde{\boldsymbol{P}}_1^{\perp}\tilde{\mathbf{z}}\right\|^2} \underset{\mathcal{H}_0}{\overset{\mathcal{H}_1}{\gtrless}} \tilde{\lambda}_G, \tag{18}$$

where $\tilde{\lambda}$ denotes the detection threshold.

B. Performance analysis

Let's begin with the full-rank waveform. Denoting $\boldsymbol{S}$ as the orthogonal complement of $\mathcal{R}(\boldsymbol{P}_1^{\perp})$ in $\mathcal{R}(\boldsymbol{P}_0^{\perp})$, we rewrite the test as

$$\frac{\left\|\boldsymbol{P}_0^{\perp}\bar{\mathbf{z}}\right\|^2}{\left\|\boldsymbol{P}_1^{\perp}\bar{\mathbf{z}}\right\|^2} = \frac{\left\|\boldsymbol{P}_1^{\perp}\bar{\mathbf{z}}\right\|^2 + \left\|\boldsymbol{P}_{\boldsymbol{S}}\bar{\mathbf{z}}\right\|^2}{\left\|\boldsymbol{P}_1^{\perp}\bar{\mathbf{z}}\right\|^2} = 1 + \frac{\left\|\boldsymbol{P}_{\boldsymbol{S}}\bar{\mathbf{z}}\right\|^2}{\left\|\boldsymbol{P}_1^{\perp}\bar{\mathbf{z}}\right\|^2}. \tag{19}$$

Let's define $X = \frac{\left\|\boldsymbol{P}_{\boldsymbol{S}}\bar{\mathbf{z}}\right\|^2}{\left\|\boldsymbol{P}_1^{\perp}\bar{\mathbf{z}}\right\|^2}$, under the null hypothesis $\mathcal{H}_0$, X represents the ratio of two independent central Chi-square random variables, with $2K_0$ and $2(M_T M_R - K_0 - 2K_1)$ degrees of freedom, respectively. Consequently, X follows a Fisher-Snedecor distribution [13, Section VIII], with a density function given by

$$f_{X|\mathcal{H}_0}(x) = \frac{1}{B\left(K_0; m\right)} x^{K_0 - 1}(1+x)^{-(m+K_0)}, \tag{20}$$

where $B\left(a; b\right)$ denotes the beta function with parameters a and b, and

$$m = M_T M_R - K_0 - 2K_1. \tag{21}$$

Under $\mathcal{H}_1$, assuming $\boldsymbol{\beta}_1 \sim \mathcal{CN}(0, \sigma_\beta^2 \boldsymbol{I}_{K_0+2K_1})$ with covariance σ_β^2, we have

$$\begin{aligned}
&\mathbb{E}\left(\|\boldsymbol{P}_{\boldsymbol{S}}\bar{\mathbf{z}}\|^2|\mathcal{H}_1\right) = \mathbb{E}\left(\|\boldsymbol{P}_{\boldsymbol{S}}\mathbf{A}_1\boldsymbol{\beta}_1 + \boldsymbol{P}_{\boldsymbol{S}}\mathbf{r}\|^2\right) \\
&= \text{Trace}\left(\mathbf{A}_1^H \mathbf{\Sigma}_x^{1/2}\boldsymbol{P}_{\boldsymbol{S}}\mathbf{\Sigma}_x^{1/2}\mathbf{A}_1\right)\sigma_\beta^2 + \sigma^2 K_0 \\
&= \text{Trace}\left(\mathbf{A}_{\text{LOS}}^H \mathbf{\Sigma}_x^{1/2}\boldsymbol{P}_0^{\perp}\mathbf{\Sigma}_x^{1/2}\mathbf{A}_{\text{LOS}}\right)\sigma_\beta^2 + \sigma^2 K_0,
\end{aligned} \tag{22}$$

the random variable X has density

$$\begin{aligned}
f_{X|\mathcal{H}_1}(x) = &\frac{1}{(1+\rho_1)B\left(K_0; m\right)}\left(\frac{x}{1+\rho_1}\right)^{K_0-1} \\
&\times\left(1+\frac{x}{1+\rho_1}\right)^{-(m+K_0)},
\end{aligned} \tag{23}$$

where

$$\rho_1 = \frac{\text{Trace}\left(\mathbf{A}_{\text{LOS}}^H \mathbf{\Sigma}_x^{1/2}\boldsymbol{P}_0^{\perp}\mathbf{\Sigma}_x^{1/2}\mathbf{A}_{\text{LOS}}\right)\sigma_\beta^2}{K_0\sigma^2}. \tag{24}$$

Then, the performance of the test can calculated:

$$P_{\text{fa}} = 1 - \frac{1}{B\left(K_0; m\right)}\sum_{i=0}^{m-1}\binom{m-1}{i}\frac{(-1)^i}{K_0+i}\left(1-\frac{1}{\lambda_G}\right)^{K_0+i}, \tag{25}$$

$$P_{\text{d}} = 1 - \frac{1}{B\left(K_0; m\right)}\sum_{i=0}^{m-1}\binom{m-1}{i}\frac{(-1)^i}{K_0+i}\left(\frac{\lambda_G-1}{\lambda_G+\rho_1}\right)^{K_0+i}. \tag{26}$$

Similarly, we can derive the theoretical performance of the detector with the rank-deficient waveform. The false alarm probability and detection probability are given by (25) and (26) with m and ρ_1 replaced by

$$\tilde{m} = JM_R - K_0 - 2K_1 \tag{27}$$

and

$$\tilde{\rho}_1 = \frac{\text{Trace}\left(\widetilde{\mathbf{A}}_{\text{LOS}}^H \mathbf{\Sigma}_s^{1/2}\widetilde{\boldsymbol{P}}_0^{\perp}\mathbf{\Sigma}_s^{1/2}\widetilde{\mathbf{A}}_{\text{LOS}}\right)\sigma_\beta^2}{K_0\sigma^2}, \tag{28}$$

respectively. This expression of probability of false alarm shows the threshold setting is feasible with no prior knowledge as to the clutter power, namely it exhibits the desirable constant false alarm rate (CFAR) property against the disturbance covariance matrix.

C. Angle estimation

When the number of paths and their corresponding angles are unknown, the matrices $\mathbf{A}_{\text{LOS}}$ and $\mathbf{A}_{\text{NLOS}}$ are not known, even in terms of their order. This makes it challenging to implement the detector. Following this, we will outline proposed angle finding technique aimed at providing the detector with the necessary information, thus rendering the test (13) implementable. To obtain the MLE of the matrices $\mathbf{A}_{\text{LOS}}$ and $\mathbf{A}_{\text{NLOS}}$, it involves addressing problem $\min_{K_0,K_1,\mathbf{A}_1\in\mathbb{C}^{M_T M_R\times(K_0+2K_1)}}\left\|\boldsymbol{P}_1^{\perp}\bar{\mathbf{z}}\right\|^2$. However, directly solving it often leads to overestimation of the model order, as larger values of K_0 and K_1 tend to minimize the objective function. So we resort to introduce the sparsity in the paths, where K_0 and K_1 are typically much smaller than $M_T M_R$, to estimate the angles and number of paths. Specifically, the problem of estimating these matrices can be formulated as:

$$\begin{aligned}
(\hat{K}_0, \hat{K}_1, \widehat{\mathbf{A}}_{\text{LOS}}, \widehat{\mathbf{A}}_{\text{NLOS}}) = &\underset{\substack{K_0,K_1,\\ \mathbf{A}_{\text{LOS}}\in\mathbb{C}^{K_0\times 1},\\ \mathbf{A}_{\text{NLOS}}\in\mathbb{C}^{2K_1\times 1}}}{\arg\min} \quad K_0 + \delta K_1 \\
\text{s.t.} \quad &\| \mathbf{z} - \mathbf{\Sigma}_x(\mathbf{A}_{\text{LOS}}\boldsymbol{\alpha} + \mathbf{A}_{\text{NLOS}}\boldsymbol{\alpha}')\|^2 \leq \epsilon^2,
\end{aligned} \tag{29}$$

where δ is the parameter characterizing the weights between K_0 and K_1. It is worth noting that for any $\mathbf{A}_1 = [\mathbf{A}_{\text{LOS}}, \mathbf{A}_{\text{NLOS}}]$, $\boldsymbol{\beta}_1 = [\boldsymbol{\alpha}^T, (\boldsymbol{\alpha}')^T]^T$ should be $(\mathbf{\Sigma}_x^{1/2}\mathbf{A}_1)^{\dagger}\bar{\mathbf{z}}$ to minimize $\| \mathbf{z} - \mathbf{\Sigma}_x(\mathbf{A}_{\text{LOS}}\boldsymbol{\alpha} + \mathbf{A}_{\text{NLOS}}\boldsymbol{\alpha}')\|^2$, so the constraints degrades to $\left\|\boldsymbol{P}_1^{\perp}\bar{\mathbf{z}}\right\|^2 \leq \epsilon^2$. The Continuous Domain Compressed Sensing method (CSCD) proposed in [10] employs an iterative procedure to solve (29). In each iteration, it initially obtains coarse estimates of the paths through grid search, followed by fine angle estimation using the Levenberg-Marquardt (LM) method. Additionally, CSCD utilizes a group-sparsity enforced structure to leverage the paired characteristic of NLOS paths and has demonstrated robust performance in multipath estimation.

Once the $\widehat{\mathbf{A}}_{\text{LOS}}$ and $\widehat{\mathbf{A}}_{\text{NLOS}}$ are estimated, the test is then utilized for the detection of $\mathcal{H}_1$ from $\mathcal{H}_0$

$$\frac{\left\|\bar{\mathbf{z}} - \mathbf{\Sigma}_x^{1/2}\widehat{\mathbf{A}}_0(\mathbf{\Sigma}_x^{1/2}\widehat{\mathbf{A}}_0)^{\dagger}\bar{\mathbf{z}}\right\|^2}{\left\|\bar{\mathbf{z}} - \mathbf{\Sigma}_x^{1/2}\widehat{\mathbf{A}}_1(\mathbf{\Sigma}_x^{1/2}\widehat{\mathbf{A}}_1)^{\dagger}\bar{\mathbf{z}}\right\|^2} \underset{\mathcal{H}_0}{\overset{\mathcal{H}_1}{\gtrless}} \lambda_G, \tag{30}$$

where $\widehat{\mathbf{A}}_0 = \widehat{\mathbf{A}}_{\mathrm{NLOS}}$ and $\widehat{\mathbf{A}}_1 = [\widehat{\mathbf{A}}_{\mathrm{LOS}}, \widehat{\mathbf{A}}_{\mathrm{NLOS}}]$.

IV. Simulations

In this section, numerical simulations are conducted to evaluate the detection performance of the full-rank and deficient-rank waveforms when the path parameters are known, as well as the estimation performance of full-rank waveforms when the path parameters are unknown.

For the detection scheme with unknown parameters, the CSCD estimation method is adopted to estimate the unknown angles, so the detector is named GLRT-CSCD for simplicity. Additionally, we adopt an Orthogonal Matching Pursuit (OMP)-based estimator [14] to provide angle estimation and introduce GLRT-OMP algorithms for the purpose of comparison. OMP is a classic on-grid method in Compressed Sensing (CS) that doesn't require grid refinement in the continuous domain, resulting in lower computational complexity. Based on our analysis of the complexity of both algorithms [10, Section V], the CSCD-based estimator, due to the addition of refined angle estimation, has a slightly higher computational complexity than the OMP-based estimator. However, it's important to note that the computational complexity of the refined estimation is independent of grid density, enabling us to reduce computational load by employing a coarser grid. The simulation parameters are set as follows:

1) Denote $\mathbf{x}_n = [x_n(1), x_n(2), \cdots, x_n(L)]^T$ as the code of n-th transmitter across L epoch, we normalize the transmission power of each transmit antenna, i.e. $\mathbf{x}_n^H \mathbf{x}_n = 1$. The space-time code, with a length of $L = 256$, are generated through random phase encoding with constant modulus. The TBF matrix for the deficient-rank waveform is constructed based on the known LOS path angles, where $J = K_0$, i.e., $\mathbf{F} = \sqrt{M_T/K_0}\mathbf{A}_T^*(\boldsymbol{\theta})$.
2) The number of transmitting and receiving elements in the MIMO array are set as $M_T = 10$ and $M_R = 10$, respectively. The noise follows a Gaussian distribution with variance $\sigma^2 = 1$. We set $\boldsymbol{\beta}_1 \sim \mathcal{CN}(0, \sigma_\beta^2 \boldsymbol{I}_{K_0+2K_1})$ and define the signal-to-noise ratio (SNR) as σ_β^2/σ^2.
3) The angle space ranging from $-90°$ to $90°$ is discretized with a step size of $2°$ to obtain the grids. Both the OMP-based and CSCD-based estimators have a maximum iteration limit of $T = 10$. The stopping criterion parameters are defined as $\epsilon = \sqrt{\sigma^2 M_T M_R}$ and $\delta = 1$.
4) The false alarm rate for detection is set to 10^{-4}, and the number of independent trials used for detection is 10^4. The Monte Carlo trial count for estimation experiments is set to 2000.

Firstly, we would like to assess the influence of varying values for K_0 and K_1 on detection performance, assuming known path parameters. In Fig. 1, with K_1 fixed at 1, we observe an improvement in detection performance for both waveforms as the K_0 increases. Notably, the rank-deficient waveform benefits from the gain introduced by the formation of transmit beams, resulting in $\tilde{\rho}_1$ being significantly larger than ρ_1 of the full-rank waveform. This leads to a significant enhancement in LOS detection performance compared to the full-rank waveform. Intuitively, this can be explained as the rank-deficient waveform, equipped with the TBF method, concentrating energy on the LOS path, thereby enhancing detection performance.

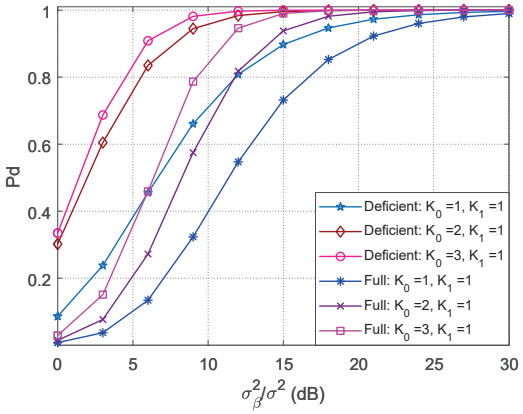

Fig. 1: P_{d} versus σ_β^2/σ^2 with different K_0.

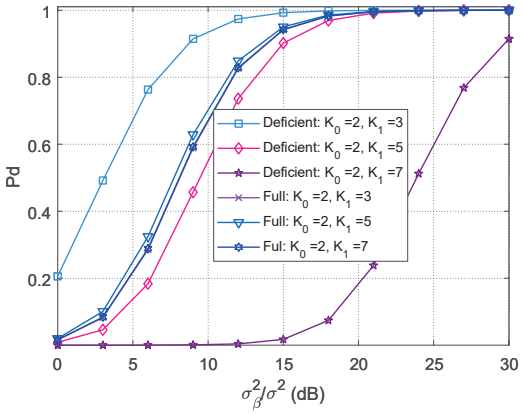

Fig. 2: P_{d} versus σ_β^2/σ^2 with different K_1.

In Fig. 2, we set $K_0 = 2$ and investigate the influence of increasing K_1. Different trends are observed. For the rank-deficient waveform, although performance is notably superior to the full-rank waveform when $K_1 = 3$, it gradually decreases with an increase in K_1. In the case of $K_1 = 7$, its performance is significantly inferior to the full-rank. This is because the full-rank waveform having a DOF m much larger than the rank-deficient waveform's DOF $\tilde{m}$. With the ability to fully utilize the available degrees of freedom to generate as many diversity branches as possible in the signal space, the full-rank waveform exhibits superior LOS detection performance in scenarios with dense multipaths (larger K_1).

When the angles of paths are unknown, generating the TBF matrix to employ the rank-deficient waveform becomes unimplementable due to a lack of prior information on LOS angles and the number of paths. So we validate the detection and estimation performance of LOS in full-rank waveforms. Firstly, in Fig. 3, we set the path number $K_0 = 2, K_1 = 3$ and evaluate the root-mean-squared-error (RMSE) [10] of the

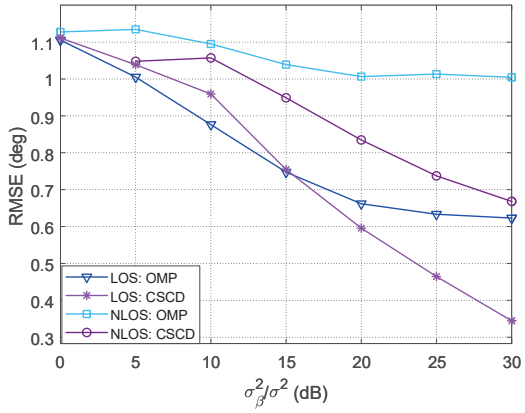

Fig. 3: RMSE versus σ_β^2/σ^2 with different estimation methods.

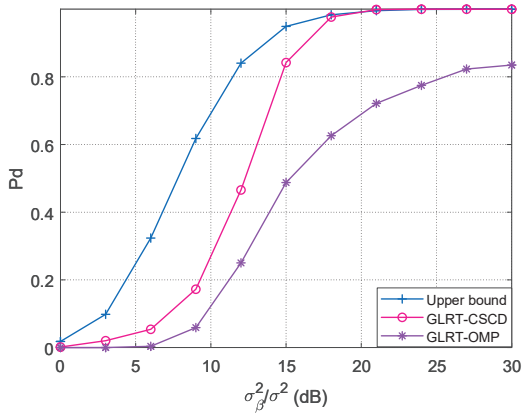

Fig. 4: P_{d} versus σ_β^2/σ^2 with different estimation methods.

angle estimation algorithms. We refer to the RMSEs conditioned on the correct path estimation, with a path considered correctly estimated if its estimation error is smaller than the grid resolution. As expected, we find that both NLOS and LOS have better estimation accuracy when using the CSCD method for continuous-domain angle estimation compared to using the OMP method on a discrete grid. This difference in estimation performance is reflected in GLRT, as seen in Fig. 4, where GLRT-CSCD consistently outperforms GLRT-OMP in detection performance.

V. Conclusion

In this paper, we investigate localization using a monostatic ISAC system in the presence of multipaths. We formulated the LOS detection as a binary detection problem and derived the corresponding GLRT detectors for two waveforms: the full-rank and rank-deficient waveforms. The theoretical detection performance of the proposed GLRT has been analyzed under perfect angle estimation. We find that the rank-deficient waveform can benefit from accumulation advantages through TBF, enhancing detection performance in low-density NLOS scenarios. The full-rank waveform, with its higher degree of freedom, exhibits relatively stable detection performance across various scenarios. Particularly, it demonstrates superior LOS detection performance compared to the rank-deficient waveform in dense multipath scenarios.

In the case of unknown path parameters, we propose CSCD method for angle estimation method based on the full-rank waveform. The proposed CSCD method, which performs LOS and NLOS angle estimation in the continuous domain, exhibits superior estimation accuracy compared to methods such as OMP that operate on discrete grid points. Simulation results indicate that the GLRT-CSCD outperforms the GLRT-OMP.

VI. Acknowledgment

The work of M. Lops was partially supported by the European Union under the Italian National Recovery and Resilience Plan (PNRR) of Next Generation EU, partnership on "Telecommunications of the Future" (PE00000001 – program "RESTART" – E63C22002040007)

References

[1] F. Liu, L. Zheng, Y. Cui, C. Masouros, A. P. Petropulu, H. Griffiths, and Y. C. Eldar, "Seventy years of radar and communications: The road from separation to integration," *IEEE Signal Processing Magazine*, vol. 40, no. 5, pp. 106–121, 2023.

[2] S. Sun, A. P. Petropulu, and H. V. Poor, "MIMO radar for advanced driver-assistance systems and autonomous driving: Advantages and challenges," *IEEE Signal Processing Magazine*, vol. 37, no. 4, pp. 98–117, 2020.

[3] S. Lu, F. Liu, and L. Hanzo, "The Degrees-of-Freedom in Monostatic ISAC Channels: NLoS Exploitation vs. Reduction," *IEEE Transactions on Vehicular Technology*, vol. 72, no. 2, pp. 2643–2648, 2023.

[4] P. Kumari, J. Choi, N. González-Prelcic, and R. W. Heath, "IEEE 802.11ad-based radar: An approach to joint vehicular communication-radar system," *IEEE Transactions on Vehicular Technology*, vol. 67, no. 4, pp. 3012–3027, 2018.

[5] R. Feng, E. D. Greef, M. Rykunov, H. Sahli, S. Pollin, and A. Bourdoux, "Multipath ghost recognition for indoor MIMO radar," *IEEE Transactions on Geoscience and Remote Sensing*, vol. 60, pp. 1–10, 2022.

[6] Q. Shi, L. Liu, and S. Zhang, "Joint data association, NLOS mitigation, and clutter suppression for networked device-free sensing in 6G cellular network," in *ICASSP 2023 - 2023 IEEE International Conference on Acoustics, Speech and Signal Processing (ICASSP)*, 2023, pp. 1–5.

[7] X. Zhao, J. Li, and Q. Guo, "Robust target localization in distributed mimo radar with nonconvex lp minimization and iterative reweighting," *IEEE Communications Letters*, pp. 1–1, 2023.

[8] J. Yu and Y. Wang, "Deep learning-based multipath DoAs estimation method for mmwave Massive MIMO systems in low SNR," *IEEE Transactions on Vehicular Technology*, vol. 72, no. 6, pp. 7480–7490, 2023.

[9] F. Engels, M. Wintermantel, and P. Heidenreich, "Automotive MIMO radar angle estimation in the presence of multipath," in *2017 European Radar Conference (EURAD)*, 2017, pp. 82–85.

[10] L. Zheng, J. Long, M. Lops, F. Liu, and X. Hu, "Identification of ghost targets for automotive radar in the presence of multipath," p. arXiv:2309.13585, 2023.

[11] L. Zheng, M. Lops, X. Wang, and E. Grossi, "Joint design of overlaid communication systems and pulsed radars," *IEEE Transactions on Signal Processing*, vol. 66, no. 1, pp. 139–154, 2018.

[12] E. Fishler, A. Haimovich, R. Blum, L. Cimini, D. Chizhik, and R. Valenzuela, "Spatial diversity in radars—models and detection performance," *IEEE Transactions on Signal Processing*, vol. 54, no. 3, pp. 823–838, 2006.

[13] L. Scharf and B. Friedlander, "Matched subspace detectors," *IEEE Transactions on Signal Processing*, vol. 42, no. 8, pp. 2146–2157, 1994.

[14] A. Aich and P. Palanisamy, "On-grid DOA estimation method using orthogonal matching pursuit," in *2017 International Conference on Signal Processing and Communication (ICSPC)*, 2017, pp. 483–487.